ELSEVIER

Physica A 316 (2002) 87–114

PHYSICA A

www.elsevier.com/locate/physa

Multifractal detrended fluctuation analysis of nonstationary time series

Jan W. Kantelhardt[a,b,*], Stephan A. Zschiegner[a], Eva Koscielny-Bunde[c,a], Shlomo Havlin[d,a], Armin Bunde[a], H. Eugene Stanley[b]

[a] *Institut für Theoretische Physik III, Justus-Liebig-Universität Giessen, Heinrich-Buff-Ring 16, D-35392 Giessen, Germany*

[b] *Department of Physics, Center for Polymer Studies, Boston University, Boston, MA 02215, USA*

[c] *Potsdam Institute for Climate Impact Research, P.O. Box 60 12 03, D-14412 Potsdam, Germany*

[d] *Department of Physics and Gonda-Goldschmied-Center for Medical Diagnosis, Bar-Ilan University, Ramat-Gan 52900, Israel*

Abstract

We develop a method for the multifractal characterization of nonstationary time series, which is based on a generalization of the detrended fluctuation analysis (DFA). We relate our multifractal DFA method to the standard partition function-based multifractal formalism, and prove that both approaches are equivalent for stationary signals with compact support. By analyzing several examples we show that the new method can reliably determine the multifractal scaling behavior of time series. By comparing the multifractal DFA results for original series with those for shuffled series we can distinguish multifractality due to long-range correlations from multifractality due to a broad probability density function. We also compare our results with the wavelet transform modulus maxima method, and show that the results are equivalent.

PACS: 05.45.Tp; 05.40.−a

Keywords: Multifractal formalism; Scaling; Nonstationarities; Time series analysis; Long-range correlations; Broad distributions; Detrended fluctuation analysis

* Corresponding author. Institut für Theoretische Physik III, Justus-Liebig-Universität Giessen, Heinrich-Buff-Ring 16, 35392 Giessen, Germany.

E-mail address: jan.w.kantelhardt@theo.physik.uni-giessen.de (J.W. Kantelhardt).

0378-4371/02/$ - see front matter
PII: S0378-4371(02)01383-3

1. Introduction

In recent years the detrended fluctuation analysis (DFA) method [1,2] has become a widely used technique for the determination of (mono-) fractal scaling properties and the detection of long-range correlations in noisy, nonstationary time series [3–6]. It has successfully been applied to diverse fields such as DNA sequences [1,2,7,8], heart rate dynamics [9–13], neuron spiking [14,15], human gait [16], long-time weather records [17–19], cloud structure [20], geology [21], ethnology [22], economics time series [23–25], and solid state physics [26,27]. One reason to employ the DFA method is to avoid spurious detection of correlations that are artifacts of nonstationarities in the time series.

Many records do not exhibit a simple monofractal scaling behavior, which can be accounted for by a single scaling exponent. In some cases, there exist crossover (time-) scales $s_\times$ separating regimes with different scaling exponents [4,5], e.g. long-range correlations on small scales $s \ll s_\times$ and another type of correlations or uncorrelated behavior on larger scales $s \gg s_\times$. In other cases, the scaling behavior is more complicated, and different scaling exponents are required for different parts of the series [6]. This occurs, e.g., when the scaling behavior in the first half of the series differs from the scaling behavior in the second half. In even more complicated cases, such different scaling behavior can be observed for many interwoven fractal subsets of the time series. In this case a multitude of scaling exponents is required for a full description of the scaling behavior, and a multifractal analysis must be applied.

In general, two different types of multifractality in time series can be distinguished: (i) Multifractality due to a broad probability density function for the values of the time series. In this case the multifractality cannot be removed by shuffling the series. (ii) Multifractality due to different long-range (time-) correlations of the small and large fluctuations. In this case the probability density function of the values can be a regular distribution with finite moments, e.g. a Gaussian distribution. The corresponding shuffled series will exhibit nonmultifractal scaling, since all long-range correlations are destroyed by the shuffling procedure. If both kinds of multifractality are present, the shuffled series will show weaker multifractality than the original series.

The simplest type of multifractal analysis is based upon the standard partition function multifractal formalism, which has been developed for the multifractal characterization of normalized, stationary measures [28–31]. Unfortunately, this standard formalism does not give correct results for nonstationary time series that are affected by trends or that cannot be normalized. Thus, in the early 1990s an improved multifractal formalism has been developed, the wavelet transform modulus maxima (WTMM) method [32–39], which is based on wavelet analysis and involves tracing the maxima lines in the continuous wavelet transform over all scales. Here, we propose an alternative approach based on a generalization of the DFA method. This multifractal DFA (MF-DFA) does not require the modulus maxima procedure, and hence does not involve more effort in programming than the conventional DFA.

The paper is organized as follows: In Section 2 we describe the MF-DFA method in detail and show that the scaling exponents determined via the MF-DFA method are identical to those obtained by the standard multifractal formalism based on partition

functions. In Section 3 we introduce several multifractal models, where the scaling exponents can be calculated exactly, and compare these analytical results with the numerical results obtained by MF-DFA. In Section 4, we show how the comparison of the MF-DFA results for original series with the MF-DFA results for shuffled series can be used to determine the type of multifractality in the series. In Section 5, we compare the results of the MF-DFA with those obtained by the WTMM method for nonstationary series and discuss the performance of both methods for multifractal time series analysis.

2. Multifractal DFA

2.1. Description of the method

The generalized multifractal DFA (MF-DFA) procedure consists of five steps. The first three steps are essentially identical to the conventional DFA procedure (see, e.g. [1–6]). Let us suppose that x_k is a series of length N, and that this series is of compact support. The support is defined as the set of the indices k with nonzero values x_k, and it is compact if $x_k = 0$ for an insignificant fraction of the series only. The value of $x_k = 0$ is interpreted as having no value at this k.

Note that we are *not* discussing the fractal or multifractal features of the plot of the time series in a two-dimensional graph. The reason is that the time axis and the value axis are not equivalent. The graph is neither monofractal nor multifractal structure in a strict sense (but rather a self-affine structure), because the scaling properties depend on the direction. Hence, we analyze time series as one-dimensional structures with values assigned to each point and consider the multifractality of these values. Since real time series always have finite length N, we explicitly want to determine the multifractality of finite series, and we are not discussing the limit for $N \to \infty$ here.

- *Step* 1: Determine the "profile"

$$Y(i) \equiv \sum_{k=1}^{i} [x_k - \langle x \rangle], \quad i = 1, \ldots, N \; . \tag{1}$$

Subtraction of the mean $\langle x \rangle$ is not compulsory, since it would be eliminated by the later detrending in the third step.

- *Step* 2: Divide the profile $Y(i)$ into $N_s \equiv \mathrm{int}(N/s)$ nonoverlapping segments of equal length s. Since the length N of the series is often not a multiple of the considered time scale s, a short part at the end of the profile may remain. In order not to disregard this part of the series, the same procedure is repeated starting from the opposite end. Thereby, $2N_s$ segments are obtained altogether.
- *Step* 3: Calculate the local trend for each of the $2N_s$ segments by a least-square fit of the series. Then determine the variance

$$F^2(v,s) \equiv \frac{1}{s} \sum_{i=1}^{s} \{Y[(v-1)s + i] - y_v(i)\}^2 \tag{2}$$

for each segment v, $v = 1,\ldots,N_s$ and

$$F^2(v,s) \equiv \frac{1}{s}\sum_{i=1}^{s}\{Y[N-(v-N_s)s+i]-y_v(i)\}^2 \tag{3}$$

for $v = N_s+1,\ldots,2N_s$. Here, $y_v(i)$ is the fitting polynomial in segment v. Linear, quadratic, cubic, or higher order polynomials can be used in the fitting procedure (conventionally called DFA1, DFA2, DFA3, ...) [1,2,13]. Since the detrending of the time series is done by the subtraction of the polynomial fits from the profile, different order DFA differ in their capability of eliminating trends in the series. In (MF-)DFAm [mth order (MF-)DFA] trends of order m in the profile (or, equivalently, of order $m-1$ in the original series) are eliminated. Thus a comparison of the results for different orders of DFA allows one to estimate the type of the polynomial trend in the time series [4,5].

- *Step* 4: Average over all segments to obtain the qth order fluctuation function

$$F_q(s) \equiv \left\{\frac{1}{2N_s}\sum_{v=1}^{2N_s}[F^2(v,s)]^{q/2}\right\}^{1/q}, \tag{4}$$

where, in general, the index variable q can take any real value (for $q=0$, see step 5). For $q=2$, the standard DFA procedure is retrieved. We are interested in how the generalized q dependent fluctuation functions $F_q(s)$ depend on the time scale s for different values of q. Hence, we must repeat steps 2 to 4 for several time scales s. It is apparent that $F_q(s)$ will increase with increasing s. Of course, $F_q(s)$ depends on the DFA order m. By construction, $F_q(s)$ is only defined for $s \geqslant m+2$.

- *Step* 5: Determine the scaling behavior of the fluctuation functions by analyzing log–log plots $F_q(s)$ versus s for each value of q. Several examples of this procedure will be shown in Section 3. If the series x_i are long-range power-law correlated, $F_q(s)$ increases, for large values of s, as a power-law,

$$F_q(s) \sim s^{h(q)}. \tag{5}$$

For very large scales, $s > N/4$, $F_q(s)$ becomes statistically unreliable because the number of segments N_s for the averaging procedure in step 4 becomes very small. Thus, we usually exclude scales $s > N/4$ from the fitting procedure to determine $h(q)$. Besides that, systematic deviations from the scaling behavior in Eq. (5), which can be corrected, occur for very small scales $s \approx 10$. In general, the exponent $h(q)$ in Eq. (5) may depend on q. For stationary time series, $h(2)$ is identical to the well-known Hurst exponent H (see, e.g. [28]). Thus, we will call the function $h(q)$ generalized Hurst exponent.

The value of $h(0)$, which corresponds to the limit $h(q)$ for $q \to 0$, cannot be determined directly using the averaging procedure in Eq. (4) because of the diverging exponent. Instead, a logarithmic averaging procedure has to be employed,

$$F_0(s) \equiv \exp\left\{\frac{1}{4N_s}\sum_{v=1}^{2N_s}\ln[F^2(v,s)]\right\} \sim s^{h(0)}. \tag{6}$$

Note that $h(0)$ cannot be defined for time series with fractal support, where $h(q)$ diverges for $q \to 0$.

For monofractal time series with compact support, $h(q)$ is independent of q, since the scaling behavior of the variances $F^2(v,s)$ is identical for all segments v, and the averaging procedure in Eq. (4) will give just this identical scaling behavior for all values of q. Only if small and large fluctuations scale differently, there will be a significant dependence of $h(q)$ on q: If we consider positive values of q, the segments v with large variance $F^2(v,s)$ (i.e., large deviations from the corresponding fit) will dominate the average $F_q(s)$. Thus, for positive values of q, $h(q)$ describes the scaling behavior of the segments with large fluctuations. On the contrary, for negative values of q, the segments v with small variance $F^2(v,s)$ will dominate the average $F_q(s)$. Hence, for negative values of q, $h(q)$ describes the scaling behavior of the segments with small fluctuations.

Usually the large fluctuations are characterized by a smaller scaling exponent $h(q)$ for multifractal series than the small fluctuations. This can be understood from the following arguments: For the maximum scale $s = N$ the fluctuation function $F_q(s)$ is independent of q, since the sum in Eq. (4) runs over only two identical segments ($N_s \equiv [N/s] = 1$). For smaller scales $s \ll N$ the averaging procedure runs over several segments, and the average value $F_q(s)$ will be dominated by the $F^2(v,s)$ from the segments with small (large) fluctuations if $q < 0$ ($q > 0$). Thus, for $s \ll N$, $F_q(s)$ with $q < 0$ will be smaller than $F_q(s)$ with $q > 0$, while both become equal for $s = N$. Hence, if we assume an homogeneous scaling behavior of $F_q(s)$ following Eq. (5), the slope $h(q)$ in a log–log plot of $F_q(s)$ with $q < 0$ versus s must be larger than the corresponding slope for $F_q(s)$ with $q > 0$. Thus, $h(q)$ for $q < 0$ will usually be larger than $h(q)$ for $q > 0$.

However, the MF-DFA method can only determine *positive* generalized Hurst exponents $h(q)$, and it already becomes inaccurate for strongly anti-correlated signals when $h(q)$ is close to zero. In such cases, a modified (MF-)DFA technique has to be used. The most simple way to analyze such data is to integrate the time series before the MF-DFA procedure. Hence, we replace the *single* summation in Eq. (1), which is describing the profile from the original data x_k, by a *double* summation

$$\tilde{Y}(i) \equiv \sum_{k=1}^{i} [Y(k) - \langle Y \rangle] \,. \tag{7}$$

Following the MF-DFA procedure as described above, we obtain generalized fluctuation functions $\tilde{F}_q(s)$ described by a scaling law as in Eq. (5), but with larger exponents $\tilde{h}(q) = h(q) + 1$,

$$\tilde{F}_q(s) \sim s^{\tilde{h}(q)} = s^{h(q)+1} \,. \tag{8}$$

Thus, the scaling behavior can be accurately determined even for $h(q)$ which are smaller than zero (but larger than -1) for some values of q. We note that $\tilde{F}_q(s)/s$ corresponds to $F_q(s)$ in Eq. (5). If we do not subtract the average values in each step of the summation in Eq. (7), this summation leads to quadratic trends in the profile $\tilde{Y}(i)$. In this case we must employ at least the second order MF-DFA to eliminate these artificial trends.

2.2. Relation to standard multifractal analysis

For stationary, normalized series defining a measure with compact support the multifractal scaling exponents $h(q)$ defined in Eq. (5) are directly related, as shown below, to the scaling exponents $\tau(q)$ defined by the standard partition function-based multifractal formalism.

Suppose that the series x_k of length N is a stationary, positive, and normalized sequence, i.e., $x_k \geqslant 0$ and $\sum_{k=1}^{N} x_k = 1$. Then the detrending procedure in step 3 of the MF-DFA method is not required, since no trend has to be eliminated. Thus, the DFA can be replaced by the standard fluctuation analysis (FA), which is identical to the DFA except for a simplified definition of the variance for each segment v, $v = 1, \ldots, N_s$, in step 3 [see Eq. (2)]:

$$F_{\mathrm{FA}}^2(v,s) \equiv [Y(vs) - Y((v-1)s)]^2 \,. \tag{9}$$

Inserting this simplified definition into Eq. (4) and using Eq. (5), we obtain

$$\left\{ \frac{1}{2N_s} \sum_{v=1}^{2N_s} |Y(vs) - Y((v-1)s)|^q \right\}^{1/q} \sim s^{h(q)} \,. \tag{10}$$

For simplicity we can assume that the length N of the series is an integer multiple of the scale s, obtaining $N_s = N/s$ and therefore

$$\sum_{v=1}^{N/s} |Y(vs) - Y((v-1)s)|^q \sim s^{qh(q)-1} \,. \tag{11}$$

This already corresponds to the multifractal formalism used, e.g. in Refs. [29,31]. In fact, a hierarchy of exponents H_q similar to our $h(q)$ has been introduced based on Eq. (11) in Ref. [29].

In order to relate the MF-DFA also to the standard textbook box counting formalism [28,30], we employ the definition of the profile in Eq. (1). It is evident that the term $Y(vs) - Y((v-1)s)$ in Eq. (11) is identical to the sum of the numbers x_k within each segment v of size s. This sum is known as the box probability $p_s(v)$ in the standard multifractal formalism for normalized series x_k,

$$p_s(v) \equiv \sum_{k=(v-1)s+1}^{vs} x_k = Y(vs) - Y((v-1)s) \,. \tag{12}$$

The scaling exponent $\tau(q)$ is usually defined via the partition function $Z_q(s)$,

$$Z_q(s) \equiv \sum_{v=1}^{N/s} |p_s(v)|^q \sim s^{\tau(q)} \,, \tag{13}$$

where q is a real parameter as in the MF-DFA above. Sometimes $\tau(q)$ is defined with opposite sign (see, e.g. [28]).

Using Eq. (12) we see that Eq. (13) is identical to Eq. (11), and obtain analytically the relation between the two sets of multifractal scaling exponents,

$$\tau(q) = qh(q) - 1 \,. \tag{14}$$

Thus, we have shown that $h(q)$ defined in Eq. (5) for the MF-DFA is directly related to the classical multifractal scaling exponents $\tau(q)$.

Another way to characterize a multifractal series is the singularity spectrum $f(\alpha)$, that is related to $\tau(q)$ via a Legendre transform [28,30],

$$\alpha = \tau'(q) \quad \text{and} \quad f(\alpha) = q\alpha - \tau(q) \; . \tag{15}$$

Here, α is the singularity strength or Hölder exponent, while $f(\alpha)$ denotes the dimension of the subset of the series that is characterized by α. Using Eq. (14), we can directly relate α and $f(\alpha)$ to $h(q)$,

$$\alpha = h(q) + qh'(q) \quad \text{and} \quad f(\alpha) = q[\alpha - h(q)] + 1 \; . \tag{16}$$

3. Four illustrative examples

3.1. Example 1: monofractal uncorrelated and long-range correlated series

As a first example we apply the MF-DFA method to monofractal series with compact support, for which the generalized Hurst exponent $h(q)$ is expected to be independent of q,

$$h(q) = H \quad \text{and} \quad \tau(q) = qH - 1 \; . \tag{17}$$

Such series have been discussed in the context of conventional DFA in several studies before, see, e.g. [4–6]. Long-range correlated random numbers are usually generated by the Fourier transform method, see, e.g. [28,40]. Using this method we can generate long-range anti-correlated ($0 < H < 0.5$), uncorrelated ($H = 0.5$), or (positively) long-range correlated ($0.5 < H < 1$) series. The latter are characterized by a power-law decay of the autocorrelation function $C(s) \equiv \langle x_k x_{k+s} \rangle \sim s^{-\gamma}$ for large scales s with $\gamma = 2 - 2H$ if the series is stationary. Alternatively, all stationary long-range correlated series can be characterized by the power-law decay of their power spectra, $S(f) \sim f^{-\beta}$ with frequency f and $\beta = 2H - 1$. Note that H corresponds to the Hurst exponent of the integrated series here. Uncorrelated data are characterized by $C(s) = 0$ and $S(f) = \text{const}$, while $C(s) \sim s^{-\gamma}$ with $\gamma \geqslant 1$ (also leading to $H = 0.5$) is usually considered as short-range correlation.

Fig. 1 shows the generalized fluctuation functions $F_q(s)$ for all three types of monofractal series ($H = 0.75, 0.5, 0.25$) and several q values. On large scales s, we observe the expected power-law scaling behavior according to Eq. (5), which corresponds to straight lines in the log–log plot. In Fig. 1(d), the scaling exponents $h(q)$ determined from the slopes of these straight lines are shown versus q. Although a slight q dependence is observable, the values of $h(q)$ are always very close to the H of the generated series that has been analyzed. The degree of the q dependence observed for this monofractal series allows to estimate the usual fluctuation of $h(q)$ to be expected for monofractal series in general.

Next, we analyze multifractal series for which $\tau(q)$ can be calculated exactly, and compare the numerical results with the expected scaling behavior.

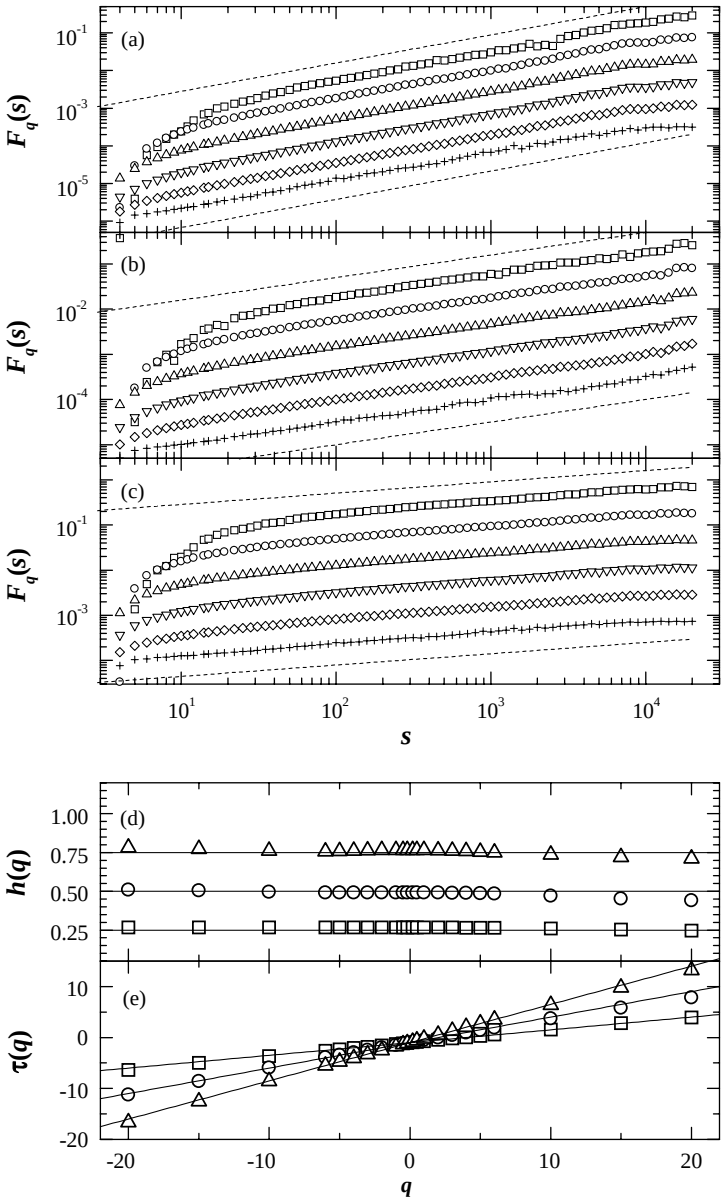

Fig. 1. The MF-DFA fluctuation functions $F_q(s)$ are shown versus the scale s in log–log plots for (a) long-range correlated monofractal series with $H = 0.75$, (b) uncorrelated random series with $H = 0.5$ (white noise), and (c) long-range anti-correlated series with $H = 0.25$. The different symbols correspond to the different values of the exponent q in the generalized averaging procedure, $q = -10$ (□), -2 (○), -0.2 (△), $+0.2$ (▽), $+2$ (◇), and $q = +10$ (+). MF-DFA2 has been employed, and the curves have been shifted by multiple factors of 4 for clarity. The straight dashed lines have the corresponding slopes H and are shown for comparison. Part (d) shows the q dependence of the asymptotic scaling exponent $h(q)$ determined by fits in the regime $200 < s < 5000$ for $H = 0.25$ (□), 0.5 (○), and 0.75 (△). The very weak dependence on q is consistent with monofractal scaling. In part (e) the q dependence of $\tau(q)$, $\tau(q) = qh(q) - 1$, is shown. Series of length $N = 65536$ were analyzed.

3.2. Example 2: binomial multifractal series

In the binomial multifractal model [28–30], a series of $N = 2^{n_{\max}}$ numbers k with $k = 1, \ldots, N$ is defined by

$$x_k = a^{n(k-1)}(1-a)^{n_{\max}-n(k-1)} , \tag{18}$$

where $0.5 < a < 1$ is a parameter and $n(k)$ is the number of digits equal to 1 in the binary representation of the index k, e.g. $n(13) = 3$, since 13 corresponds to binary 1101.

The scaling exponents $\tau(q)$ can be calculated straightforwardly. According to Eqs. (12) and (18) the box probability $p_{2s}(v)$ in the vth segment of size $2s$ is given by

$$p_{2s}(v) = p_s(2v-1) + p_s(2v) = [(1-a)/a + 1]\, p_s(2v) = p_s(2v)/a .$$

Thus, according to Eqs. (13) and (18),

$$\begin{aligned} Z_q(s) &= \sum_{v=1}^{N/s} [p_s(v)]^q = \sum_{v=1}^{N/2s} [p_s(2v-1)]^q + [p_s(2v)]^q \\ &= \left[\frac{(1-a)^q}{a^q} + 1\right] \sum_{v=1}^{N/2s} [p_s(2v)]^q \\ &= [(1-a)^q + a^q] \sum_{v=1}^{N/2s} [p_{2s}(v)]^q = [(1-a)^q + a^q] Z_q(2s) \end{aligned}$$

and according to Eqs. (13) and (14),

$$\tau(q) = \frac{-\ln[a^q + (1-a)^q]}{\ln(2)} , \tag{19}$$

$$h(q) = \frac{1}{q} - \frac{\ln[a^q + (1-a)^q]}{q \ln(2)} . \tag{20}$$

Note that $\tau(0) = -1$ as required. There is a strong nonlinear dependence of $\tau(q)$ upon q, indicating multifractality. The same information is comprised in the q dependence of $h(q)$. The asymptotic values are $h(q) \to -\ln(a)/\ln(2)$ for $q \to +\infty$ and $h(q) \to -\ln(1-a)/\ln(2)$ for $q \to -\infty$. They correspond to the scaling behavior of the largest and weakest fluctuations, respectively. Note that $h(q)$ becomes independent of q in the asymptotic limit, while $\tau(q)$ approaches linear q dependences.

Fig. 2 shows the MF-DFA fluctuation functions $F_q(s)$ for the binomial multifractal model with $a = 0.75$. The results for MF-DFA1 and MF-DFA4 are compared in parts (a) and (b). Fig. 2(c) shows the corresponding slopes $h(q)$ for three values of a together with the exact results obtained from Eq. (20). The numerical results are in good agreement with Eq. (20), showing that the MF-DFA correctly detects the multifractal scaling exponents. Figs. 2(d) and (e) show the corresponding exponents $\tau(q) = qh(q) - 1$ [see Eq. (14)] and the corresponding $f(\alpha)$ spectrum calculated from $h(q)$ using the modified Legendre transform (16). Both are also in good agreement with Eq. (19). We have also checked that the results for the binomial multifractal model remain unchanged if the double summation technique [see Eq. (7)] is applied. We obtain

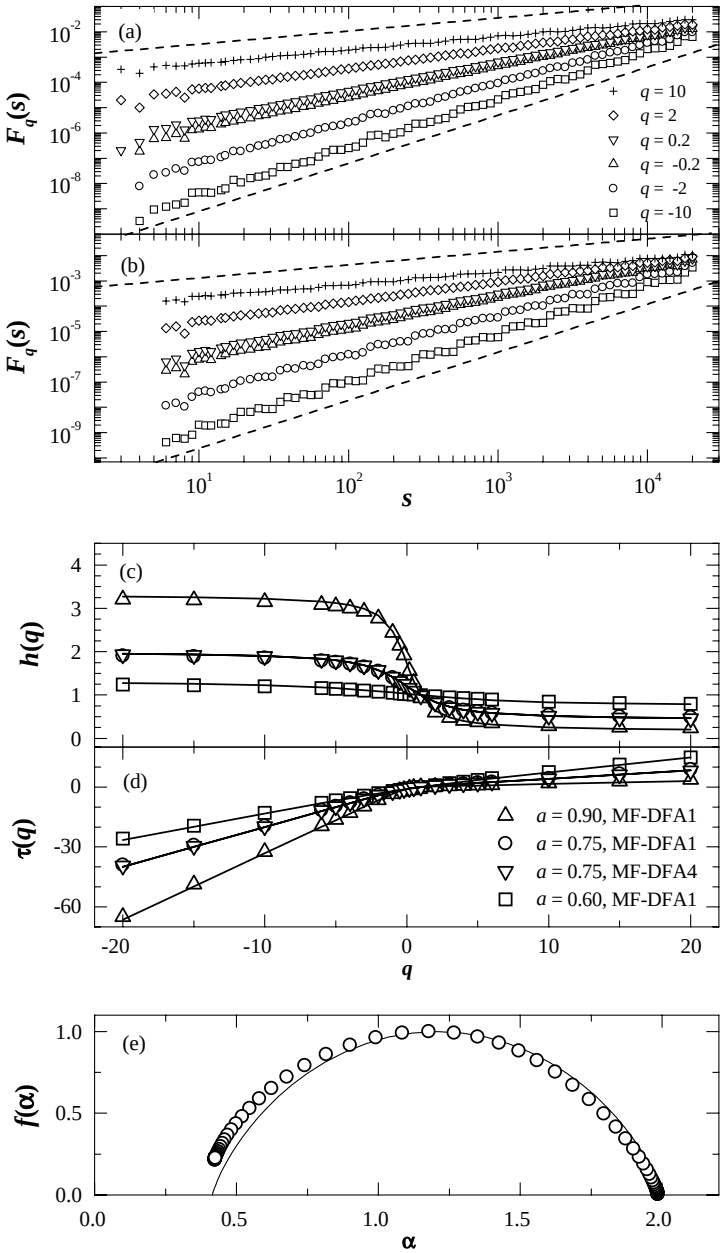

Fig. 2. The MF-DFA fluctuation functions $F_q(s)$ are shown versus the scale s in log–log plots for the binomial multifractal model with $a = 0.75$ (a) for MF-DFA1 and (b) for MF-DFA4. The symbols are the same as for Fig. 1. The straight dashed lines have the corresponding theoretical slopes $h(-10) = 1.90$ and $h(+10)=0.515$ and are shown for comparison. In part (c) the q dependence of the generalized Hurst exponent $h(q)$ determined by fits in the regime $50 < s < 500$ is shown for MF-DFA1 and $a = 0.9$ (△), $a = 0.75$ (○), and $a = 0.6$ (□), as well as for MF-DFA4 and $a = 0.75$ (▽). Parts (d) and (e) show the corresponding exponents $\tau(q)$ and the corresponding singularity spectrum $f(\alpha)$ for $a = 0.75$ determined by the modified Legendre transform (16), respectively. The lines are the theoretical values obtained from Eq. (20). Series of length $N = 65536$ were analyzed.

slopes $\tilde{h}(q) = h(q) + 1$ as expected in Eq. (8). Note that there is no need to use this modification, except if $h(q)$ is close to zero or has negative values.

3.3. Example 3: dyadic random cascade model with log-Poisson distribution

For another independent test of the MF-DFA, we employ an algorithm based on random cascades on wavelet dyadic trees proposed in Refs. [41,42] (see also [43]). This algorithm builds a random multifractal series by specifying its discrete wavelet coefficients $c_{n,m}$, defined recursively,

$$c_{1,1} = 1, \quad c_{n,2m-1} = W c_{n-1,m}, \quad c_{n,2m} = W c_{n-1,m} \ ,$$

where $n = 2,\ldots,n_{\max}$ (with $N = 2^{n_{\max}}$) and $m = 1,\ldots,2^{n-2}$. The values of W are taken from a log-Poisson distribution, $|W| = \exp(P \ln \delta + \gamma)$, where P is Poisson distributed with $\langle P \rangle = \lambda$. There are three independent parameters, λ, δ, and γ. Inverse wavelet transform is applied to create the multifractal random series x_k once the wavelet coefficients $c_{n,m}$ are known,

$$x_k = \sum_{n=1}^{n_{\max}} \sum_{m=1}^{2^{n-1}} c_{n,m} \psi_{n,m}(k) \ , \tag{21}$$

where $\psi_{n,m}(k)$ is a set of wavelets forming an orthonormal wavelet basis. Here, we employ the Haar wavelets, $\psi_{n,m}(k) \equiv 2^{(n-n_{\max}-1)/2} \psi[2^{n-n_{\max}-1}k - m]$ with $\psi(x) \equiv 1$ for $0 < x \leqslant 0.5$, $\psi(x) \equiv -1$ for $0.5 < x \leqslant 1$ and $\psi(x) \equiv 0$ otherwise. For this model the multifractal scaling exponents are given by [41,42]

$$\tau(q) = \frac{\lambda(1-\delta^q) - \gamma q}{\ln 2} - 1 \ , \tag{22}$$

$$h(q) = [\lambda(1-\delta^q) - \gamma q]/(q \ln 2) \ . \tag{23}$$

Fig. 3 shows the MF-DFA fluctuation functions $F_q(s)$ for the dyadic random cascade model. The numerically determined slopes $h(q)$ for three sets of parameters are compared with the exact results obtained from Eq. (23) and the good agreement shows that the MF-DFA correctly detects the multifractal scaling exponents. Large deviations occur only for very small moments ($q < -10$), indicating that the range of q values should not exceed -10.

3.4. Example 4: uncorrelated multifractal series with power-law distribution function

The examples discussed in the previous three subsections were based on series involving long-range correlations. In the present example we want to apply the MF-DFA method to an uncorrelated series, that nevertheless exhibits multifractal scaling behavior due to the broad distribution of its values. We denote by $P(x)$ the probability density function of the values x_k in the series. The distribution $P(x)$ does not affect the multifractality of a series on large scales s, if all moments

$$\langle |x|^q \rangle \equiv \int_{-\infty}^{\infty} |x|^q P(x) \, \mathrm{d}x \tag{24}$$

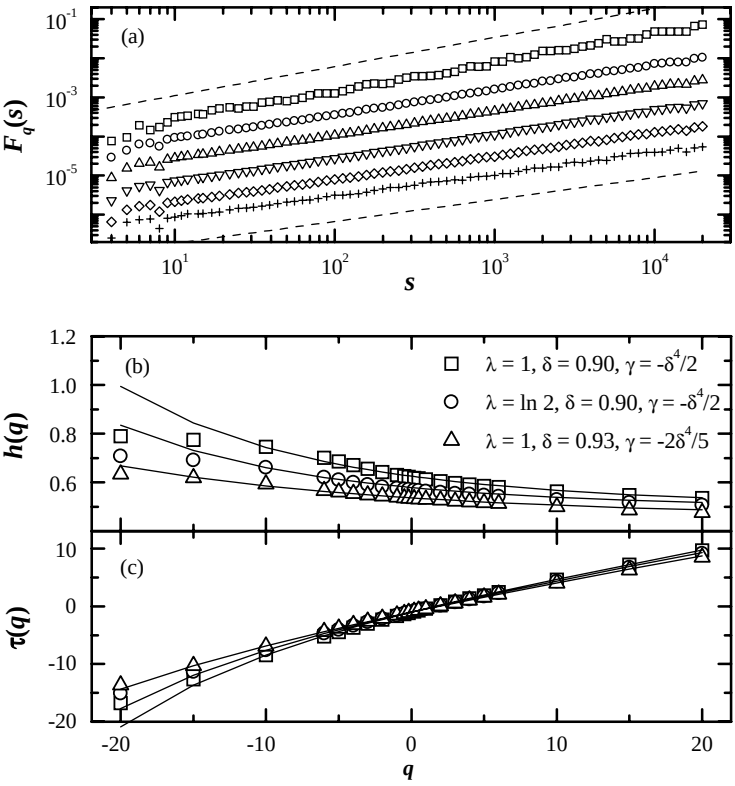

Fig. 3. (a) The MF-DFA2 fluctuation functions $F_q(s)$ are shown versus the scale s in a log–log plot for the dyadic random cascade model with log-Poisson distribution with parameters $\lambda = 1$, $\delta = 0.9$, and $\gamma = -\delta^4/2$. The symbols are the same as for Fig. 1. The dashed straight lines have the theoretical slopes $h(-10) = 0.743$ and $h(+10) = 0.567$ and are shown for comparison. (b) The q dependence of the generalized Hurst exponent $h(q)$ determined by fits is shown for MF-DFA2 and different parameters (see legend). The lines are the theoretical values obtained from Eq. (23). In part (c) $\tau(q) = qh(q) - 1$ is shown. Series of length $N = 65536$ were analyzed.

are finite. Here we choose a (normalized) power-law probability distribution function,

$$P(x) = \alpha x^{-(\alpha+1)} \quad \text{for } 1 \leqslant x < \infty \quad \text{with } \alpha > 0 \tag{25}$$

and $P(x) = 0$ for $x < 1$, where already the second moment diverges if $\alpha \leqslant 2$. Thus, the study definitely has to be restricted to *finite* series in this example. If $\alpha \leqslant 2$, the series exhibits multifractal scaling behavior on all scales. Note, that Eq. (25) becomes identical to a Levy distribution of class α for large values of x. The parameter α is not related to the Hölder exponent α in Eq. (15). The scaling properties of random walks with Levy distributed steps (Levy flights and Levy walks) have been analyzed in Refs. [44–46]. The multifractal nature of Levy processes has been investigated in Refs. [47,48].

In order to derive the multifractal spectrum, let us consider s uncorrelated random numbers r_k, $k=1,\ldots,s$, distributed homogeneously in the interval $[0,1]$. Obviously, the typical value of the minimum of the numbers, $r_{\min}(s) \equiv \min_{k=1}^{s} r_k$, will be $r_{\min}(s)=1/s$. It can be easily shown that the numbers r_k are transformed into numbers x_k distributed according to the power-law probability distribution function (25) by $r_k \to x_k = r_k^{-1/\alpha}$. Thus, the typical value of the maximum of the x_k will be $x_{\max}(s) \equiv \max_{k=1}^{s} x_k = [r_{\min}(s)]^{-1/\alpha} = s^{1/\alpha}$.

If $\alpha \leqslant 2$, the fluctuations of the profile $Y(i)$ [Eq. (1)] and the corresponding DFA variance $F^2(v,s)$ [Eq. (2)] will be dominated by the square of the largest value $x_{\max}^2(s)= s^{2/\alpha}$ in the segment of s numbers, since the second moment of the distribution (25) diverges. Now the whole series consists of $N_s \equiv \mathrm{int}(N/s)$ segments of length s and not just of one segment. For some segments v, $[F^2(v,s)]^{1/2}$ is larger than its typical value $x_{\max}(s) = s^{1/\alpha}$, since the maximum within the whole series of length N is $x_{\max}(N) = N^{1/\alpha}$. In order to calculate $F_q(s)$ [Eq. (4)], we need to take into account the whole distribution $P_s(y)$ of the values $y \equiv [F^2(v,s)]^{1/2}$. Since each of the maxima in the N_s segments corresponds to an actual number x_k and these x_k are random numbers from the power-law distribution (25), it becomes obvious, that the distribution of the maxima will have the same form, i.e., $P_s(y) \sim P(x=y)$ for large y. Small values of y are excluded because of the maximum procedure, but the large x_k values are very likely to be identical to the maxima of the corresponding segments. Since the smallest maxima for segments of length s are of the order of $x_{\max}(s)=s^{1/\alpha}$, the lower cutoff for $P_s(y)$ must be proportional to $s^{1/\alpha}$. From the normalization condition $\int_{As^{1/\alpha}}^{\infty} P_s(y)\,\mathrm{d}y = 1$ (with an unimportant prefactor $A<1$) we get

$$P_s(y) = A^{\alpha}\alpha s y^{-(\alpha+1)} . \tag{26}$$

Now $F_q(s)$ [Eq. (4)] can be calculated by integration from the minimum value $As^{1/\alpha}$ of $y \equiv [F^2(v,s)]^{1/2}$ to the maximum value $N^{1/\alpha}$. For $s \ll N$ we obtain

$$F_q(s) \sim \left[\int_{As^{1/\alpha}}^{N^{1/\alpha}} y^q P_s(y)\,\mathrm{d}y\right]^{1/q}$$

$$\sim \left|A^{\alpha} s N^{q/\alpha-1} - A^q s^{q/\alpha}\right|^{1/q} \sim \begin{cases} s^{1/q} & (q>\alpha) \\ s^{1/\alpha} & (q<\alpha) \end{cases} .$$

Comparing with Eq. (5), we finally get

$$h(q) \sim \begin{cases} 1/q & (q>\alpha) \\ 1/\alpha & (q \leqslant \alpha) \end{cases} . \tag{27}$$

Note that $\tau(q)$ follows a linear q dependence, $\tau(q)=q/\alpha-1$ for $q<\alpha$, while it is equal to zero for $q>\alpha$ according to Eq. (14). Hence, the series of uncorrelated power-law distributed values has rather bi-fractal [48] instead of multifractal properties. Since $h(2)=\frac{1}{2}$ holds exactly for all values of α, it is not possible to recognize the multifractality due to the broad power-law distribution of the values if only the conventional DFA is applied. The second moment shows just the uncorrelated behavior of the values. In a very recent preprint [46] this behavior has been interpreted as a failure of the

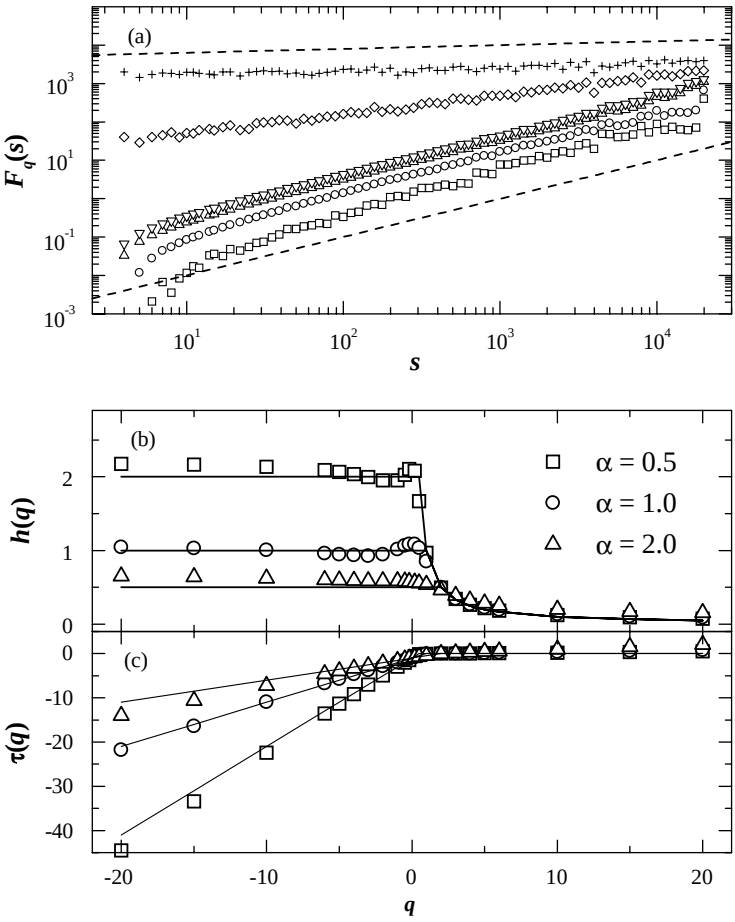

Fig. 4. (a) The modified and rescaled MF-DFA3 fluctuation functions $\tilde{F}_q(s)/s$ (corresponding to $F_q(s)$) are shown versus the scale s in a log–log plot for a series of independent numbers with a power-law probability density distribution $P(x) \sim x^{-(\alpha+1)}$ with $\alpha = 1$. The symbols are the same as for Fig. 1. The straight dashed lines have the corresponding theoretical slopes $h(-10) = 1$ and $h(+10) = 0.1$ and are shown for comparison. (b) The q dependence of the generalized Hurst exponent $h(q) = \tilde{h}(q) - 1$ determined by fits on large scales s is shown for MF-DFA3 and $\alpha = 0.5$ (□), 1.0 (○), and 2.0 (△). The lines are the theoretical values obtained from Eq. (27). In part (c) the corresponding $\tau(q)$ is shown. The broad distribution of the values leads to multifractality (bi-fractality) in all three cases. Series of length $N = 65536$ were analyzed.

DFA and corresponding nondetrending methods for series with a broad distribution, and another method to determine the exponent $1/\alpha$ has been proposed. We believe that a multifractal description with more than one exponent is required to characterize this kind of series, and thus any method calculating just one exponent will be insufficient for a full characterization.

Fig. 4(a) shows the MF-DFA3 fluctuation functions for series of independent random numbers $x_k \in [1, \infty)$ distributed according to Eq. (25) with $\alpha = 1$. Since the scaling

exponents $h(q)$ become very close to zero asymptotically for large positive values of q according to Eq. (27), we must use the modified MF-DFA technique involving the double sum as described in the last paragraph of Section 2.1. Hence, for this technical reason, $\tilde{F}_q(s)/s$ is calculated instead of $F_q(s)$. The corresponding slopes $\tilde{h}(q) - 1$ are identical to $h(q)$, see Eq. (8). In Fig. 4(b) the slopes $h(q)$ for series with α=0.5, 1.0, and 2.0 are compared with the theoretical result Eq. (27), and nice agreement is observed.

4. Comparison of the multifractality for original and shuffled series

4.1. Distinguishing the two types of multifractality

As already mentioned in the introduction, two different types of multifractality in time series can be distinguished. Both of them require a multitude of scaling exponents for small and large fluctuations. (i) Multifractality of a time series can be due to a broad probability density function for the values of the time series, and (ii) multifractality can also be due to different long-range correlations for small and large fluctuations.

In general, the example discussed in Section 3.4, the uncorrelated multifractal series with a power-law probability density function, is of type (i), while the examples discussed in Sections 3.1–3.3 are of type (ii), where the probability density function of the values is a regular distribution with finite moments. More exactly speaking, the example of the binomial multifractal series (Section 3.2) can also show multifractality due to a broad probability density function for the values x_k. If the parameter a is chosen to be very close to one or if very long series are considered, corresponding to large values of $n_{\max}$, the minimum value in the series, $(1-a)^{n_{\max}}$, will be very small compared with the maximum value $a^{n_{\max}}$ [see Eq. (18)]. In this case the log-binomial probability density function will become broad, approaching a log-normal form. Since the scaling behavior of uncorrelated log-normal distributed series corresponds to the multifractal scaling behavior observed in the example of uncorrelated power-law distributed series with $\alpha = 2$ (see Section 3.4), distribution multifractality [type (i)] will occur in addition to the correlation multifractality [type (ii)]. For the series with $a = 0.75$ and $N = 8192$ ($n_{\max} = 13$) considered in Section 3.2, we observe only type (ii) multifractality caused by long-range correlations.

Now we would like to distinguish between these two types of multifractality. The most easy way to do so is by analyzing also the corresponding randomly shuffled series. In the shuffling procedure the values are put into random order, and thus all correlations are destroyed. Hence the shuffled series from multifractals of type (ii) will exhibit simple random behavior, $h_{\text{shuf}}(q) = 0.5$, i.e., nonmultifractal scaling like in Fig. 1(b). For multifractals of type (i), on the contrary, the original $h(q)$ dependence is not changed, $h(q) = h_{\text{shuf}}(q)$, since the multifractality is due to the probability density, which is not affected by the shuffling procedure. If both kinds of multifractality are present in a given series, the shuffled series will show weaker multifractality than the original one.

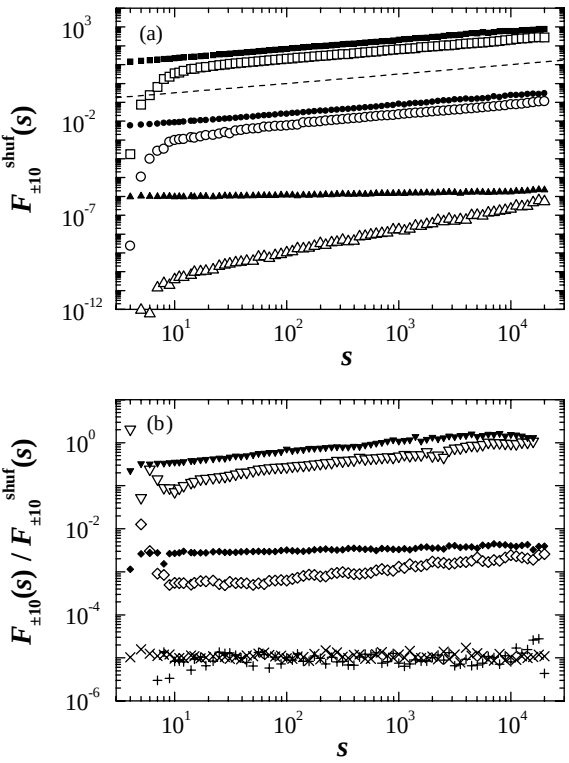

Fig. 5. (a) The MF-DFA fluctuation functions $F^{\mathrm{shuf}}_{-10}(s)$ (open symbols) and $F^{\mathrm{shuf}}_{10}(s)$ (filled symbols) are shown versus the scale s in a log–log plot for randomly shuffled series of long-range correlated series with $H = 0.75$ (□), for the dyadic random cascade model with log-Poisson distribution with parameters $\lambda = \ln 1$, $\delta = 0.9$, and $\gamma = -\delta^4/2$ (○), and for power-law distributed random numbers x_k with $P(x) \sim x^{-2}$ (△). The correlations and the multifractality are destroyed by the shuffling procedure for the first two series, but for the broadly distributed random numbers the multifractality remains. The dashed line has the slope $H = 0.5$ and is shown for comparison. (b) The ratios of the MF-DFA2 fluctuation functions $F_q(s)$ of the original series and the MF-DFA2 fluctuation functions $F^{\mathrm{shuf}}_q(s)$ of the randomly shuffled series are shown versus s for the same models as in (a), correlated series (▽), dyadic random cascade model (◇), and power-law distributed random numbers (+ for $q = -10$, × for $q = +10$). The deviations from the slope $h_{\mathrm{cor}} = 0$ indicate long-range correlations. Series of length $N = 65536$ were analyzed.

The effect of the shuffling procedure is illustrated in Fig. 5(a), where the MF-DFA2 fluctuation functions $F^{\mathrm{shuf}}_{-10}(s)$ and $F^{\mathrm{shuf}}_{10}(s)$ are shown for shuffled series for three of the multifractal examples taken from the previous section. Random behavior, $h_{\mathrm{shuf}}(q) = 0.5$, is observed for the series that were long-range correlated or generated from the dyadic random cascade model before the shuffling procedure [upper four curves in Fig. 5(a)]. In contrast, we observe the original multifractal scaling for the shuffled multifractal series with power-law probability density function $P(x) \sim x^{-2}$ [lower two curves in Fig. 5(a)]. The $h_{\mathrm{shuf}}(q)$ dependences are shown in Fig. 6, which can be compared with the corresponding slopes shown in Figs. 1(d), 3(b), and 4(b). Thus, the fluctuation

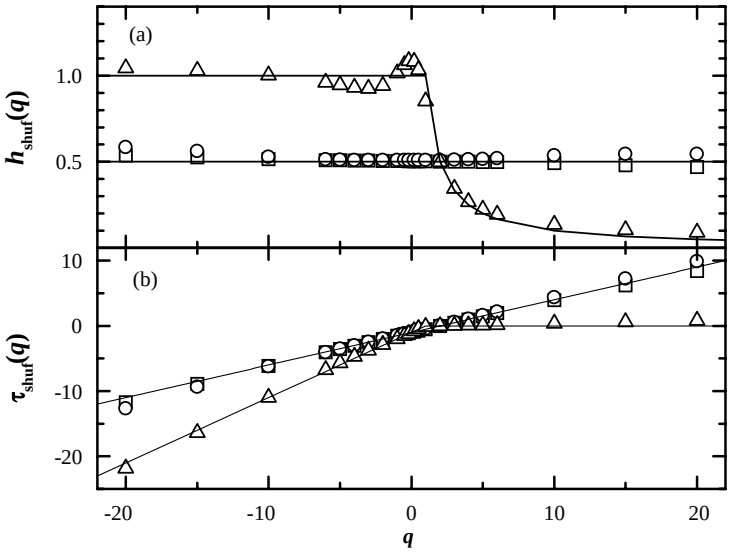

Fig. 6. (a) The q dependence of the slopes $h_{\mathrm{shuf}}(q)$ of the same models as in Fig. 5(a). The lines indicate the theoretical values: $H = 0.5$ for shuffled data with narrow distribution, and $h(q)$ from Eq. (27) for the series of numbers with a power-law probability density distribution. The symbols are the same as in Fig. 5. Part (b) shows $\tau_{\mathrm{shuf}}(q) = qh_{\mathrm{shuf}}(q) - 1$.

analysis of the shuffled series, $F_q^{\mathrm{shuf}}(s)$, directly indicates the presence of type (i) multifractality, which is due to a broad probability distribution, by deviations from $h_{\mathrm{shuf}}(q) = 0.5$.

Now we want to determine directly the magnitude of the (ii) multifractality, which is due to correlations. For that purpose we compare the fluctuation function for the original series, $F_q(s)$, with the result for the corresponding shuffled series, $F_q^{\mathrm{shuf}}(s)$. Differences between these two fluctuation functions directly indicate the presence of correlations in the original series. These differences can be observed best in a plot of the ratio $F_q(s)/F_q^{\mathrm{shuf}}(s)$ versus s. Since the anomalous scaling due to a broad probability density affects $F_q(s)$ and $F_q^{\mathrm{shuf}}(s)$ in the same way, only multifractality due to correlations will be observed in $F_q(s)/F_q^{\mathrm{shuf}}(s)$. This is illustrated in Fig. 5(b) for the same three multifractal examples as in Fig. 5(a). In order not to have increased statistical errors in the results when considering the ratio $F_q(s)/F_q^{\mathrm{shuf}}(s)$ instead of $F_q(s)$ itself, $F_q^{\mathrm{shuf}}(s)$ can be calculated by averaging over a large number of randomly shuffled series generated from the same original series.

The ratio $F_q(s)/F_q^{\mathrm{shuf}}(s)$ can also be used to eliminate systematic deviations from the expected power-law scaling behavior that occur at very small scales $s < 10$ especially for small values of q (see Figs. 1–3). A similar procedure has already been introduced for the conventional DFA recently (see Section 3.1 of Ref. [4]). Since the deviations are systematic for the MF-DFA method, they occur in both, $F_q(s)$ and $F_q^{\mathrm{shuf}}(s)$, and they should cancel in the ratio.

The scaling behavior of the ratio is

$$F_q(s)/F_q^{\mathrm{shuf}}(s) \sim s^{h(q)-h_{\mathrm{shuf}}(q)} = s^{h_{\mathrm{cor}}(q)} \,. \tag{28}$$

Note that $h(q) = h_{\mathrm{shuf}}(q) + h_{\mathrm{cor}}(q)$. If only distribution multifractality [type (i)] is present, $h(q) = h_{\mathrm{shuf}}(q)$ depends on q and $h_{\mathrm{cor}}(q) = 0$. On the other hand, deviations of $h_{\mathrm{cor}}(q)$ from zero indicate the presence of correlations, and a q dependence of $h_{\mathrm{cor}}(q)$ indicates correlation multifractality [type (ii)]. If only correlation multifractality is present, $h_{\mathrm{shuf}}(q) = 0.5$ and $h(q) = 0.5 + h_{\mathrm{cor}}(q)$. If both, distribution multifractality and correlation multifractality are present, both, $h_{\mathrm{shuf}}(q)$ and $h_{\mathrm{cor}}(q)$ depend on q.

4.2. Significance of the results

In Figs. 1–6 we have shown the results of the MF-DFA for single configurations of long time series. Now we address the significance and accuracy of the MF-DFA results for short series. How much do the numerically determined exponents $h(q)$ vary from one configuration (sample series) to the next, and how close are the average values to the theoretical values? In other words, how large are the statistical and systematical deviations of exponents practically determined by the MF-DFA for finite series? These questions are particularly important for short series, where the statistics is poor. If the values of $h(q)$ are determined inaccurately, the multifractal properties will be reported inaccurately or even false conclusions on multifractal behavior might be drawn for monofractal series.

To address the significance and accuracy of the MF-DFA results we generate, for each of the three examples considered already in Fig. 5, 100 series of length $N = 2^{13} = 8192$ and calculate $h(-10)$, $h(+10)$, $h_{\mathrm{shuf}}(-10)$, and $h_{\mathrm{shuf}}(+10)$ for each of these series. The corresponding histograms are shown in Fig. 7. For the long-range power-law correlated series with $H = 0.75$ we find the following mean values and standard deviations of the generalized Hurst exponents:

$$h(-10) = 0.80 \pm 0.03, \quad h_{\mathrm{shuf}}(-10) = 0.56 \pm 0.02 \,,$$

$$h(+10) = 0.72 \pm 0.04, \quad h_{\mathrm{shuf}}(+10) = 0.48 \pm 0.02 \,.$$

The mean values for the original series are rather close to, but not identical to the theoretical value $H = 0.75$. The mean value for $q = -10$ is about two standard deviations larger than 0.75, while the value for $q = +10$ is slightly smaller. These deviations, though, certainly *cannot* indicate multifractality, since we analyzed monofractal series. Instead, they are due to the finite, random series, where parts of the series have slightly larger and slightly smaller scaling exponent just by statistical fluctuations. By considering negative values of q we focus on the parts with small fluctuations, which are usually described by a larger scaling exponent. For positive values of q we focus on the parts with large fluctuations usually described by a smaller value of h. Thus for short records we always expect a slight difference between $h(-10)$ and $h(+10)$ even if the series are monofractal. If this difference is weak, one has to be very careful with conclusions about multifractality. Practically it is always wise to compare with generated monofractal series with otherwise similar properties before drawing conclusions

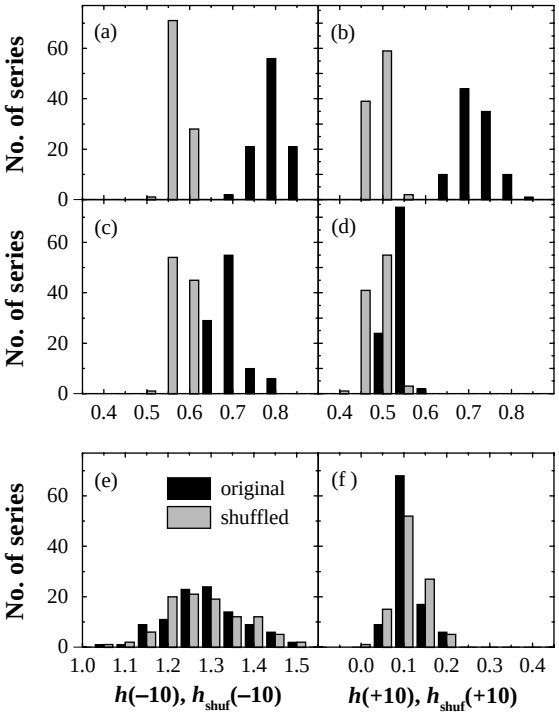

Fig. 7. (a) Histograms of the generalized Hurst exponents $h(-10)$ (black bars) and $h_{\mathrm{shuf}}(-10)$ (gray bars) for 100 generated monofractal series with $H=0.75$. The exponents have been fitted to MF-DFA2 fluctuation functions in the scaling range $400 < s < 2000$. (b) Same as (a), but for $h(+10)$ and $h_{\mathrm{shuf}}(+10)$. (c,d) Same as (a,b), but for the dyadic random cascade model with log-Poisson distribution and parameters $\lambda=\ln 1$, $\delta=0.9$, and $\gamma=-\delta^4/2$. The corresponding theoretical values are $h(-10)=0.743$ and $h(+10)=0.567$ from Eq. (23) for the original series and $h_{\mathrm{shuf}}=0.5$ for the shuffled series. From the histogram of $h(+10)$ it would be hard to draw any conclusions regarding multifractality. (e,f) Same as (a,b), but for power-law distributed random numbers with the distribution $P(x)\sim x^{-2}$. The corresponding theoretical values from Eq. (27) are $h(-10)=1$ and $h(+10)=0.1$ for the original and the shuffled series. The length of all series is $N=8192$. The figure shows that correlations and multifractality due to correlations (a–d) are eliminated by the shuffling procedure, while multifractality due to a broad distribution (e,f) remains. It further allows to estimate the statistical fluctuations in the scaling exponents $h(q)$ determined by the MF-DFA for monofractal (a,b), correlation multifractal (c,d) and distribution multifractal (e,f) series.

regarding the multifractality of a time series. In addition to the statistical fluctuations of the h values, the average $h(-10)$ is usually determined slightly too large, while $h(+10)$ is slightly too small. The same behavior is obtained if the WTMM method is used instead of the MF-DFA, as we will show in Section 5.3.

The same kind of difference is also observed for the average $h_{\mathrm{shuf}}(-10)$ and $h_{\mathrm{shuf}}(+10)$ values. After all correlations have been destroyed by the shuffling, $h_{\mathrm{shuf}}=0.5$ is expected since the probability density is Gaussian with all finite moments. The deviations from $h_{\mathrm{shuf}}=0.5$ we observe for the finite random series are characteristic

for monofractal series of this length ($N = 8192$). Only for the second moment we obtain $h_{\rm shuf}(2) = 0.5$ exactly if a sufficient number of series is considered.

For multifractal series generated from the dyadic random cascade model, Fig. 7(c,d) shows the histograms of the scaling exponents $h(-10)$, $h(+10)$, $h_{\rm shuf}(-10)$, and $h_{\rm shuf}(+10)$. Their averages and standard deviations,

$$h(-10) = 0.69 \pm 0.04, \quad h_{\rm shuf}(-10) = 0.57 \pm 0.02\ ,$$

$$h(+10) = 0.54 \pm 0.02, \quad h_{\rm shuf}(+10) = 0.48 \pm 0.02$$

have to be compared with the theoretical values from Eq. (23), $h(-10) = 0.743$ and $h(+10) = 0.567$. Surprisingly, the mean $h(-10)$ is smaller than the theoretical value in this example, but for the mean $h(+10)$ the deviation is similar to the deviation observed for the monofractal data in the previous example. Again, similar results are obtained with the WTMM method. For the shuffled series, the mean generalized Hurst exponents are practically identical to those for the shuffled monofractal series [the average $h_{\rm shuf}(-10)$ is larger by half the standard deviation], and both are evidently consistent with monofractal uncorrelated behavior, $h(q) = 0.5$, as discussed above. Hence, the series from the dyadic random cascade model show no signs of distribution multifractality and are characterized by correlation multifractality only.

The histograms of the scaling exponents for our last example, the power-law distributed random numbers with $P(x) \sim x^{-2}$, are shown in Fig. 7(e,f). The corresponding mean values and standard deviations

$$h(-10) = 1.24 \pm 0.09, \quad h_{\rm shuf}(-10) = 1.26 \pm 0.09\ ,$$

$$h(+10) = 0.11 \pm 0.03, \quad h_{\rm shuf}(+10) = 0.11 \pm 0.04$$

show obviously no differences between original and shuffled series as expected for uncorrelated series. This indicates that the multifractality is due to the broad probability density function only. The values have to be compared with $h(-10)$=1 and $h(+10)$=0.1 from Eq. (27). As usual, the average value of $h(-10)$ is too large because we analyzed short series.

5. Comparison with the WTMM method

5.1. Brief description of the WTMM method

The WTMM method [32–35] is a well-known method to investigate the multifractal scaling properties of fractal and self-affine objects in the presence of nonstationarities. For applications, see e.g. [36–39]. It is based upon the wavelet transform with continuous basis functions. One defines the wavelet-transform of a series x_k of length N by

$$W(n,s) = \frac{1}{s} \sum_{k=1}^{N} x_k \psi[(k-n)/s]\ . \tag{29}$$

Note that in this case the series x_k are analyzed directly instead of the profile $Y(i)$ defined in Eq. (1). Here, the function $\psi(x)$ is the analyzing wavelet and s is, as above, the scale parameter. The wavelet is chosen orthogonal to the possible trend. If the trend can be represented by a polynomial, a good choice for $\psi(x)$ is the mth derivative of a Gaussian, $\psi^{(m)}(x) = d^m(\mathrm{e}^{-x^2/2})/\mathrm{d}x^m$. This way, the transform eliminates trends up to $(m-1)$th order.

Now, instead of averaging over all values of $W(n,s)$, one averages, within the modulo-maxima method, only the local maxima of $|W(n,s)|$. First, one determines for a given scale s, the positions n_i of the local maxima of $|W(n,s)|$ as function of n, so that $|W(n_i-1,s)| < |W(n_i,s)| \geqslant |W(n_i+1,s)|$ for $i = 1,\ldots,i_{\max}$. Then one sums up the qth power of these maxima,

$$Z(q,s) = \sum_{i=1}^{i_{\max}} |W(n_i,s)|^q \,. \tag{30}$$

The reason for this maxima procedure is that the absolute wavelet coefficients $|W(n,s)|$ can become arbitrarily small. The analyzing wavelet $\psi(x)$ must always have positive values for some x and negative values for other x, since it has to be orthogonal to possible constant trends. Hence there are always positive and negative terms in the sum (29), and these terms might cancel. If that happens, $|W(n,s)|$ can become close to zero. Since such small terms would spoil the calculation of negative moments in Eq. (30), they have to be eliminated by the maxima procedure. In the MF-DFA, the calculation of the variances $F^2(v,s)$ in Eq. (2), i.e., the deviations from the fits, involves only positive terms under the summation. The variances cannot become arbitrarily small, and hence no maximum procedure is required for series with compact support.

In addition, the MF-DFA variances will always increase if the segment length s is increased, because the fit will always be worse for a longer segment. In the WTMM method, in contrast, the absolute wavelet coefficients $|W(n,s)|$ need not increase with increasing scale s, even if only the local maxima are considered. The values $|W(n,s)|$ might become smaller for increasing s since just more (positive and negative) terms are included in the summation (29), and these might cancel even better. Thus, an additional supremum procedure has been introduced in the WTMM method in order to keep the dependence of $Z(q,s)$ on s monotonous: If, for a given scale s, a maximum at a certain position n_i happens to be smaller than a maximum at $n_i' \approx n_i$ for a lower scale $s' < s$, then $W(n_i,s)$ is replaced by $W(n_i',s')$ in Eq. (30). There is no need for such a supremum procedure in the MF-DFA.

Often, scaling behavior is observed for $Z(q,s)$, and scaling exponents $\hat{\tau}(q)$ can be defined that describe how $Z(q,s)$ scales with s,

$$Z(q,s) \sim s^{\hat{\tau}(q)} \,. \tag{31}$$

The exponents $\hat{\tau}(q)$ characterize the multifractal properties of the series under investigation, and theoretically they are identical to the $\tau(q)$ defined in Eq. (13) [32–35] and related to $h(q)$ in Eq. (14).

5.2. Examples for series with nonstationarities

Since the WTMM method has been developed to analyze multifractal series with nonstationarities, such as trends or spikes, we will compare its performance with the performance of the MF-DFA for such nonstationary series. In Fig. 8 the MF-DFA fluctuation function $F_q(s)$ and its scaling behavior are compared with the rescaled WTMM partition sum $Z(q,s)$ for the binomial multifractal described in Section 3.2. To test the detrending capability of both methods, we have added linear as well as quadratic trends to the generated multifractal series. The trends are removed by both methods, if a sufficiently high order of detrending is employed. The deviations from the theoretical values of the scaling exponents $h(q)$ [given by Eq. (20)] are of similar size for the MF-DFA and the WTMM method. Thus, the detrending capability and the accuracy of both methods are equivalent.

We also obtain similar results for a monofractal long-range correlated series with additional spikes (outliers) that consist of large random numbers and replace a small fraction of the original series in randomly chosen positions. The spikes lead to multifractality on small scales s, while the series remains monofractal on large scales. Thus, the effects of the spikes are eliminated neither by the WTMM method nor by the MF-DFA, but both methods again give rather equivalent results.

5.3. Significance of the results

The last problem we address is a comparison of the significance of the results obtained by the MF-DFA and the WTMM method. The significance of the MF-DFA results has already been discussed in detail in Section 4.2. Here we will compare the significance of both methods for short and long series.

We begin with the significance of the results for random series involving neither correlations nor a broad distribution [as in Fig. 1(b)]. Fig. 9 shows the distribution of the multifractal Hurst exponents $h(-10)$ and $h(+10)$ calculated by the MF-DFA as well as by the WTMM using the relation $h(q) = [\hat{\tau}(q) + 1]/q$ based on Eq. (14). Similar to the results presented in Fig. 7, we have analyzed 100 generated series of uncorrelated random numbers. In addition, we compare the results for the (relatively short) series length $N = 2^{13} = 8192$ and for $N = 2^{16} = 65532$. Ideally, both, $h(-10)$ and $h(+10)$, should be equal to the Hurst exponent of the uncorrelated monofractal series, $H = 0.5$. The histograms show that similar deviations as well as remarkable fluctuations of the exponents occur for both methods, as discussed in Section 4.2 for the MF-DFA. We find the following mean values and standard deviations,

$$h(-10) = \begin{cases} 0.55 \pm 0.03 & \text{for MF-DFA } (N = 8k) \\ 0.52 \pm 0.02 & \text{for MF-DFA } (N = 64k) \\ 0.58 \pm 0.05 & \text{for WTMM } (N = 8k) \\ 0.56 \pm 0.03 & \text{for WTMM } (N = 64k) \end{cases}$$

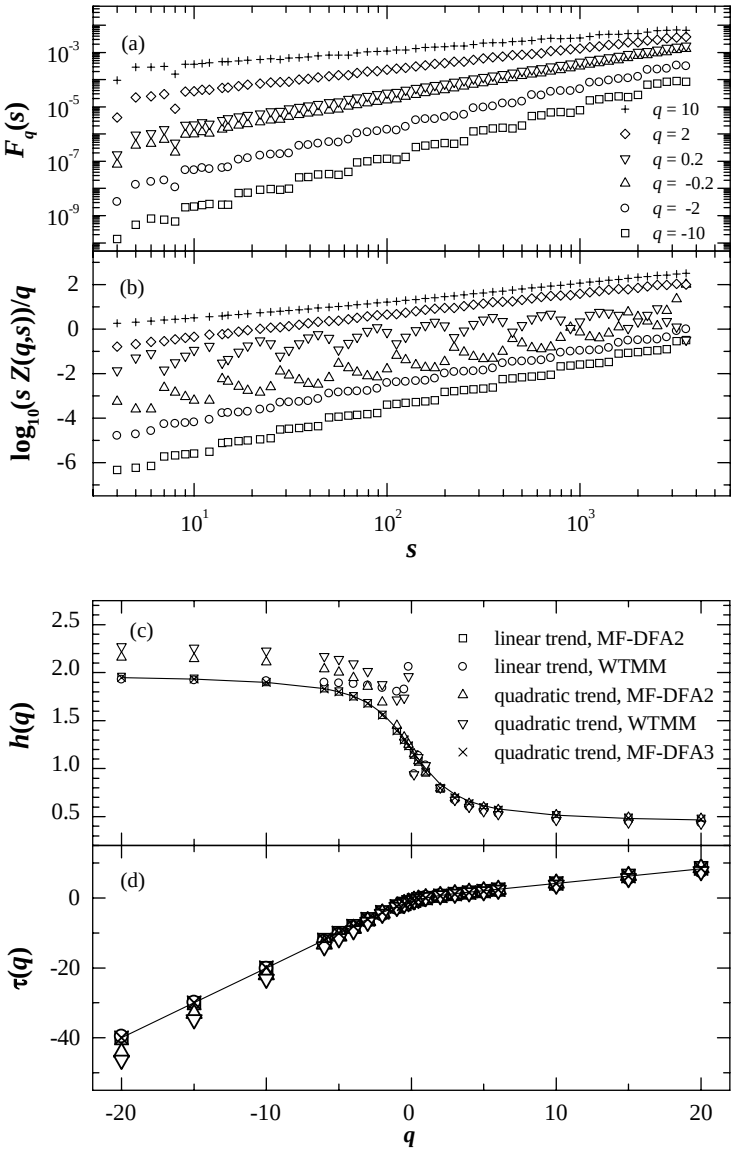

Fig. 8. (a) The MF-DFA2 fluctuation functions $F_q(s)$ are shown versus the scale s in log–log plots for the binomial multifractal model with $a = 0.75$ and an additional linear trend $x_k \to x_k + k/500N$. (b) The scaled WTMM partition functions $[sZ(q,s)]^{1/q}$ are shown for the same series and the same values of q. The symbols are the same as for Fig. 1. (c) The q dependence of the generalized Hurst exponent $h(q)$ for the generated series with linear trend for the MF-DFA2 (□) and the second order WTMM (○) methods. Corresponding results for a binomial multifractal with an additional quadratic trend are also included for MF-DFA2 (△) and second order WTMM (▽) methods. The quadratic trend causes deviations from the line indicating the theoretical values [obtained from Eq. (20)], which disappear if MF-DFA3 is employed (×). The values of $h(q)$ have been determined by fits to $F_q(s)$ and $Z(q,s)$ in the regime $50 < s < 2000$. The relation $h(q) = [\tilde{\tau}(q) + 1]/q$ from Eq. (14) has been used to convert the exponent $\tilde{\tau}(q)$ from Eq. (31) into $h(q)$. (d) The q dependence of $\tau(q)$.

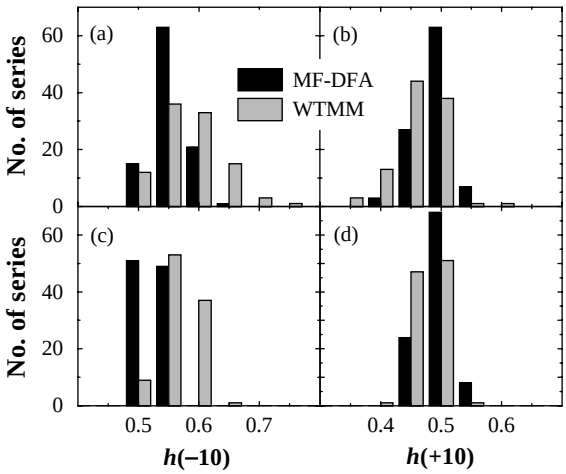

Fig. 9. (a) Histograms of the generalized Hurst exponents $h(-10)$ for 100 random uncorrelated series with $H = 0.5$. The exponents have been fitted to MF-DFA2 fluctuation functions $F_{-10}(s)$ (black bars) in the scaling range $40 < s < 2000$ and to WTMM results $Z(-10, s)$ (gray bars) in the scaling range $5 < s < 250$. We have used these different fitting regimes, since there is a factor of approximately 8 in the ratio of the segment sizes in WTMM and MF-DFA. The length of the series is $N = 8192$. The relation $h(q) = [\hat{\tau}(q) + 1]/q$ from Eq. (14) has been used to convert the exponent $\hat{\tau}(q)$ from Eq. (31) into $h(q)$. (b) Same as (a), but for $h(+10)$. (c,d) Same as (a,b), but for longer series ($N = 65536$), where statistical fluctuations are reduced. The figure shows that the MF-DFA seems to give slightly more reliable results than the WTMM method for short series and negative moments ($q = -10$), see (a). In the other cases, the performance of both methods is similar.

and

$$h(+10) = \begin{cases} 0.49 \pm 0.03 & \text{for MF-DFA } (N = 8k) \\ 0.49 \pm 0.02 & \text{for MF-DFA } (N = 64k) \\ 0.46 \pm 0.04 & \text{for WTMM } (N = 8k) \\ 0.48 \pm 0.02 & \text{for WTMM } (N = 64k) \end{cases} .$$

As already discussed in Section 4.2, the deviations of the average $h(q)$ values from $H = 0.5$ do not indicate multifractality. For the WTMM method and short series, one has to be very careful in order not to draw false conclusions from results like $h(-10) = 0.58$ and $h(+10) = 0.46$. The corresponding results of the MF-DFA are closer to the theoretical value.

Fig. 10 shows the distribution of the multifractal scaling exponents $h(-10)$ and $h(+10)$ calculated for generated multifractal series from the binomial model with $a = 0.75$ described in Section 3.2. Like for Fig. 9, 100 generated series have been analyzed for each of the histograms. Now the differences between the distributions of $h(-10)$

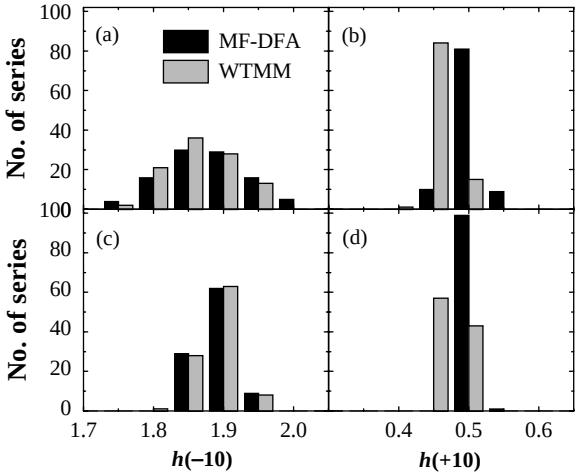

Fig. 10. Same as Fig. 9 for the binomial model with $a=0.75$. The theoretical values of the generalized Hurst exponents are $h(-10)=1.90$ and $h(+10)=0.515$ according to Eq. (20). The figure shows that our findings regarding the performance of the MF-DFA and WTMM methods for uncorrelated monofractal series in Fig. 9 also hold for multifractal series.

and $h(+10)$ are much larger, indicating multifractality. We find

$$h(-10)=\begin{cases} 1.88\pm 0.06 & \text{for MF-DFA } (N=8k) \\ 1.89\pm 0.03 & \text{for MF-DFA } (N=64k) \\ 1.86\pm 0.05 & \text{for WTMM } (N=8k) \\ 1.89\pm 0.02 & \text{for WTMM } (N=64k) \end{cases}$$

and

$$h(+10)=\begin{cases} 0.50\pm 0.02 & \text{for MF-DFA } (N=8k) \\ 0.51\pm 0.01 & \text{for MF-DFA } (N=64k) \\ 0.46\pm 0.01 & \text{for WTMM } (N=8k) \\ 0.47\pm 0.01 & \text{for WTMM } (N=64k) \end{cases}.$$

These values must be compared with the theoretical values $h(-10)=1.90$ and $h(+10)=0.515$ from Eq. (20). Again, the MF-DFA results turn out to be slightly more significant than the WTMM results. The MF-DFA seems to have slight advantages for negative q values and short series, but in the other cases the results of the two methods are rather equivalent. Besides that, the main advantage of the MF-DFA method compared with the WTMM method lies in the simplicity of the MF-DFA method.

6. Conclusion

We have generalized the DFA, widely recognized as a method to analyze the (mono-) fractal scaling properties of nonstationary time series. The MF-DFA method allows a reliable multifractal characterization of multifractal nonstationary time series. The implementation of the new method is not more difficult than that of the conventional DFA, since just one additional step, a q dependent averaging procedure, is required. We have shown for stationary signals that the generalized (multifractal) scaling exponent $h(q)$ for series with compact support is directly related to the exponent $\tau(q)$ of the standard partition function-based multifractal formalism. Further, we have shown in several examples that the MF-DFA method can reliably determine the multifractal scaling behavior of the time series, similar to the WTMM method which is a more complicated procedure for this purpose. For short series and negative moments, the significance of the results for the MF-DFA seems to be slightly better than for the WTMM method.

Contrary to the WTMM method, the MF-DFA method as described in Section 2.1 requires series of compact support, because the averaging procedure in Eq. (4) will only work if $F^2(v,s) > 0$ for all segments v. Although most time series will fulfill this prerequisite, it can be overcome by a modification of the MF-DFA technique in order to analyze data with fractal support: We restrict the sum in Eq. (4) to the local maxima, i.e., to those terms $F^2(v,s)$ that are larger than the terms $F^2(v-1,s)$ and $F^2(v+1,s)$ for the neighboring segments. By this restriction all terms $F^2(v,s)$ that are zero or very close to zero will be disregarded, and series with fractal support can be analyzed. The procedure reminds slightly of the modulus maxima procedure in the WTMM method (see Section 5.1). There is no need, though, to employ a continuously sliding window or to calculate the supremum over all lower scales for the MF-DFA, since the variances $F^2(v,s)$, which are determined by the deviations from the fit, will always increase when the segment size s is increased. In the maxima MF-DFA procedure the generalized Hurst exponent $h(q)$ defined in Eq. (5) will depend on q and even diverge for $q \to 0$ for monofractal series with noncompact support. Thus, it is more appropriate to consider the scaling exponent $\tau(q)$, calculating

$$\sum_{F^2(v-1,s)<F^2(v,s)\geqslant F^2(v+1,s)} [F^2(v,s)]^{q/2} \sim s^{\tau(q)} \,. \tag{32}$$

This extended MF-DFA procedure will also be applicable for data with fractal support.

In our future work we will apply the MF-DFA method to a range of physiological and meteorological data.

Acknowledgements

We would like to thank Yosef Ashkenazy for useful discussions and the German Academic Exchange Service (DAAD), the Deutsche Forschungsgemeinschaft (DFG), the German Israeli Foundation (GIF), the Minerva Foundation, and the NIH/National Center for Research Resources for financial support.

References

[1] C.-K. Peng, S.V. Buldyrev, S. Havlin, M. Simons, H.E. Stanley, A.L. Goldberger, Phys. Rev. E 49 (1994) 1685.
[2] S.M. Ossadnik, S.B. Buldyrev, A.L. Goldberger, S. Havlin, R.N. Mantegna, C.-K. Peng, M. Simons, H.E. Stanley, Biophys. J. 67 (1994) 64.
[3] M.S. Taqqu, V. Teverovsky, W. Willinger, Fractals 3 (1995) 785.
[4] J.W. Kantelhardt, E. Koscielny-Bunde, H.H.A. Rego, S. Havlin, A. Bunde, Physica A 295 (2001) 441.
[5] K. Hu, P.Ch. Ivanov, Z. Chen, P. Carpena, H.E. Stanley, Phys. Rev. E 64 (2001) 011114.
[6] Z. Chen, P.Ch. Ivanov, K. Hu, H.E. Stanley, Phys. Rev. E 65 (2002) 041107.
[7] S.V. Buldyrev, A.L. Goldberger, S. Havlin, R.N. Mantegna, M.E. Matsa, C.-K. Peng, M. Simons, H.E. Stanley, Phys. Rev. E 51 (1995) 5084.
[8] S.V. Buldyrev, N.V. Dokholyan, A.L. Goldberger, S. Havlin, C.-K. Peng, H.E. Stanley, G.M. Viswanathan, Physica A 249 (1998) 430.
[9] C.-K. Peng, S. Havlin, H.E. Stanley, A.L. Goldberger, Chaos 5 (1995) 82.
[10] P.Ch. Ivanov, A. Bunde, L.A.N. Amaral, S. Havlin, J. Fritsch-Yelle, R.M. Baevsky, H.E. Stanley, A.L. Goldberger, Europhys. Lett. 48 (1999) 594.
[11] Y. Ashkenazy, M. Lewkowicz, J. Levitan, S. Havlin, K. Saermark, H. Moelgaard, P.E.B. Thomsen, M. Moller, U. Hintze, H.V. Huikuri, Europhys. Lett. 53 (2001) 709.
[12] Y. Ashkenazy, P.Ch. Ivanov, S. Havlin, C.-K. Peng, A.L. Goldberger, H.E. Stanley, Phys. Rev. Lett. 86 (2001) 1900.
[13] A. Bunde, S. Havlin, J.W. Kantelhardt, T. Penzel, J.-H. Peter, K. Voigt, Phys. Rev. Lett. 85 (2000) 3736.
[14] S. Blesic, S. Milosevic, D. Stratimirovic, M. Ljubisavljevic, Physica A 268 (1999) 275.
[15] S. Bahar, J.W. Kantelhardt, A. Neiman, H.H.A. Rego, D.F. Russell, L. Wilkens, A. Bunde, F. Moss, Europhys. Lett. 56 (2001) 454.
[16] J.M. Hausdorff, S.L. Mitchell, R. Firtion, C.-K. Peng, M.E. Cudkowicz, J.Y. Wei, A.L. Goldberger, J. Appl. Physiol. 82 (1997) 262.
[17] E. Koscielny-Bunde, A. Bunde, S. Havlin, H.E. Roman, Y. Goldreich, H.-J. Schellnhuber, Phys. Rev. Lett. 81 (1998) 729.
[18] K. Ivanova, M. Ausloos, Physica A 274 (1999) 349.
[19] P. Talkner, R.O. Weber, Phys. Rev. E 62 (2000) 150.
[20] K. Ivanova, M. Ausloos, E.E. Clothiaux, T.P. Ackerman, Europhys. Lett. 52 (2000) 40.
[21] B.D. Malamud, D.L. Turcotte, J. Stat. Plan. Infer. 80 (1999) 173.
[22] C.L. Alados, M.A. Huffman, Ethnology 106 (2000) 105.
[23] R.N. Mantegna, H.E. Stanley, An Introduction to Econophysics, Cambridge University Press, Cambridge, 2000.
[24] Y. Liu, P. Gopikrishnan, P. Cizeau, M. Meyer, C.-K. Peng, H.E. Stanley, Phys. Rev. E 60 (1999) 1390.
[25] N. Vandewalle, M. Ausloos, P. Boveroux, Physica A 269 (1999) 170.
[26] J.W. Kantelhardt, R. Berkovits, S. Havlin, A. Bunde, Physica A 266 (1999) 461.
[27] N. Vandewalle, M. Ausloos, M. Houssa, P.W. Mertens, M.M. Heyns, Appl. Phys. Lett. 74 (1999) 1579.
[28] J. Feder, Fractals, Plenum Press, New York, 1988.
[29] A.-L. Barabási, T. Vicsek, Phys. Rev. A 44 (1991) 2730.
[30] H.-O. Peitgen, H. Jürgens, D. Saupe, Chaos and Fractals, Springer, New York, 1992 (Appendix B).
[31] E. Bacry, J. Delour, J.F. Muzy, Phys. Rev. E 64 (2001) 026103.
[32] J.F. Muzy, E. Bacry, A. Arneodo, Phys. Rev. Lett. 67 (1991) 3515.
[33] J.F. Muzy, E. Bacry, A. Arneodo, Int. J. Bifurcat. Chaos 4 (1994) 245.
[34] A. Arneodo, E. Bacry, P.V. Graves, J.F. Muzy, Phys. Rev. Lett. 74 (1995) 3293.
[35] A. Arneodo, et al., in: A. Bunde, J. Kropp, H.-J. Schellnhuber (Eds.), The Science of Disaster: Climate Disruptions, Market Crashes, and Heart Attacks, Springer, Berlin, 2002, pp. 27–102.
[36] P.Ch. Ivanov, L.A.N. Amaral, A.L. Goldberger, S. Havlin, M.G. Rosenblum, Z.R. Struzik, H.E. Stanley, Nature 399 (1999) 461.
[37] L.A.N. Amaral, P.Ch. Ivanov, N. Aoyagi, I. Hidaka, S. Tomono, A.L. Goldberger, H.E. Stanley, Y. Yamamoto, Phys. Rev. Lett. 86 (2001) 6026.

[38] A. Arneodo, N. Decoster, S.G. Roux, Eur. Phys. J. B 15 (2000) 567, 739, and 765.
[39] A. Silchenko, C.K. Hu, Phys. Rev. E 63 (2001) 041105.
[40] H.A. Makse, S. Havlin, M. Schwartz, H.E. Stanley, Phys. Rev. E 53 (1996) 5445.
[41] A. Arneodo, E. Bacry, J.F. Muzy, J. Math. Phys. 39 (1998) 4142.
[42] A. Arneodo, S. Manneville, J.F. Muzy, Europhys. J. B 1 (1998) 129.
[43] Y. Ashkenazy, S. Havlin. P.Ch. Ivanov, C.K. Peng, V. Schulte-Frohlinde, H.E. Stanley, unpublished (cond-mat/0111396).
[44] M.F. Shlesinger, B.J. West, J. Klafter, Phys. Rev. Lett. 58 (1987) 1100.
[45] S. Havlin, Y. Ben Avraham, Diffusion and Reactions in Fractals and Disordered Systems, Cambridge University Press, Cambridge, 2000, p. 48, and references therein.
[46] N. Scafetta, P. Grigolini, unpublished (cond-mat/0202008).
[47] S. Jaffard, Probab. Theory Relat. 114 (1999) 207.
[48] H. Nakao, Phys. Lett. A 266 (2000) 282.